Research Article | Vol. 27, No. 9 | 29 Apr 2019 | OPTICS EXPRESS 12855
Optics EXPRESS

Highly sensitive, broadband microwave frequency identification using a chip-based Brillouin optoelectronic oscillator

ZIHANG ZHU,[1,2,3] MORITZ MERKLEIN,[1,2,*] DUK-YONG CHOI,[4] KHU VU,[4] PAN MA,[4] STEVEN J. MADDEN,[4] AND BENJAMIN J. EGGLETON[1,2]

[1]*Institute of Photonics and Optical Science (IPOS), School of Physics, The University of Sydney, NSW 2006, Australia*
[2]*The University of Sydney Nano Institute (Sydney Nano), The University of Sydney, NSW 2006, Australia*
[3]*The Faculty of Automation & Information Engineering, Xi'an University of Technology, Xi'an 710048, China*
[4]*Laser Physics Centre, Australian National University, Canberra, Australian Capital Territory 2601, Australia*
[*]*moritz.merklein@sydney.edu.au*

Abstract: Detection and frequency estimation of radio frequency (RF) signals are critical in modern RF systems, including wireless communication and radar. Photonic techniques have made huge progress in solving the problem imposed by the fundamental trade-off between detection range and accuracy. However, neither fiber-based nor integrated photonic RF signal detection and frequency estimation systems have achieved wide range and low error with high sensitivity simultaneously in a single system. In this paper, we demonstrate the first Brillouin opto-electronic oscillator (B-OEO) based on on-chip stimulated Brillouin scattering (SBS) to achieve RF signal detection. The broad tunability and narrowband amplification of on-chip SBS allow for the wide-range and high-accuracy detection. Feeding the unknown RF signal into the B-OEO cavity amplifies the signal which is matched with the oscillation mode to detect low-power RF signals. We are able to detect RF signals from 1.5 to 40 GHz with power levels as low as −67 dBm and a frequency accuracy of ± 3.4 MHz. This result paves the way to compact, fully integrated RF detection and channelization.

1. Introduction

With the rapid increase in the carrier frequency of transmitted RF signals and the complexity of today's electromagnetic environment, detecting and precisely estimating the frequency of RF signals over a broad frequency range and with high accuracy becomes more and more important for many applications, such as wireless communication [1], RF channelization [2], radio astronomy [3] and many more. For these applications, the RF signals are often in a cluttered environment with very low power after long-distance transmission, demanding high detection sensitivity for the receivers. However, it is difficult to detect and measure the frequency of a low-power RF signal with wide-range and high-accuracy simultaneously using modern electrical techniques [4].

Photonic techniques have recently been introduced in RF signal detection due to the advantages of high frequency, broad bandwidth and immunity to electromagnetic interference [5–17]. Initially, photonic RF signal detection and frequency estimation systems were based on fiber optics components [5–8]. They have shown the potential for a broad frequency range using a Sagnac loop [5], a high detection sensitivity based on fiber Brag grating [6] or fiber-based SBS [7], and a low detection error based on amplified fiber-optic recirculating delay loop and broadband incoherent light source [8]. However, these optimum performances are obtained separately using different schemes and no single scheme has met all the performance

#361789 https://doi.org/10.1364/OE.27.012855
Journal © 2019 Received 6 Mar 2019; revised 12 Apr 2019; accepted 13 Apr 2019; published 22 Apr 2019

Optics EXPRESS

requirements simultaneously. In order to improve the stability, compactness, and unit cost of the fiber-based system, recently, several integrated photonic RF signal detection and frequency estimation schemes have been proposed [9–14]. However, most on-chip RF signal detection systems to date have a frequency measurement range lower than 10 GHz [9–11]. In order to expand the bandwidth of the system, a linear amplitude-to-frequency mapping system based on a waveguide Bragg grating on silicon was proposed and demonstrated [12], which has the frequency measurement range of 30 GHz. However, the frequency estimation error is as high as 755 MHz, which is attributed to the degradation of the noise figure of the photonic link. In [13], on-chip four-wave mixing (FWM) was used to detect RF signals with the bandwidth of 40 GHz. However, the frequency estimation error is still 318.9 MHz, and increases as the bandwidth of the system increases. In order to circumvent the trade-off between the bandwidth and accuracy, a photonic microwave frequency measurement scheme using an on-chip stimulated Brillouin scattering (SBS) based microwave photonic notch filter scheme was proposed [14] and a frequency range of 9-38 GHz with an ultra-low error of 1 MHz was achieved. However, the minimum frequency that can be measured is 9 GHz, which is limited by the on-chip SBS frequency shift. Furthermore, the sensitivity of this scheme is limited as the unknown RF signal that is to be measured is used to generate optical sidebands which act as the SBS pump.

Neither fiber-based nor integrated photonic RF signal detection and frequency estimation systems have achieved simultaneously wide range and low error with high sensitivity in a single system. Incorporating these features in one integrated on-chip platform means great improvement for an advanced RF detection system with reduced size weight and power consumption, which is crucial for deployment in mobile platforms.

In this paper, we experimentally demonstrate a microwave frequency identification scheme that detects RF signals as low as −67 dBm with 1.5-40 GHz frequency range and ± 3.4 MHz frequency uncertainty using a B-OEO based on on-chip SBS. The results show the possibilities for establishing high performance fully integrated RF signal detection system. Furthermore, the selective amplification and filtering of B-OEO facilitate future systems for RF channelization.

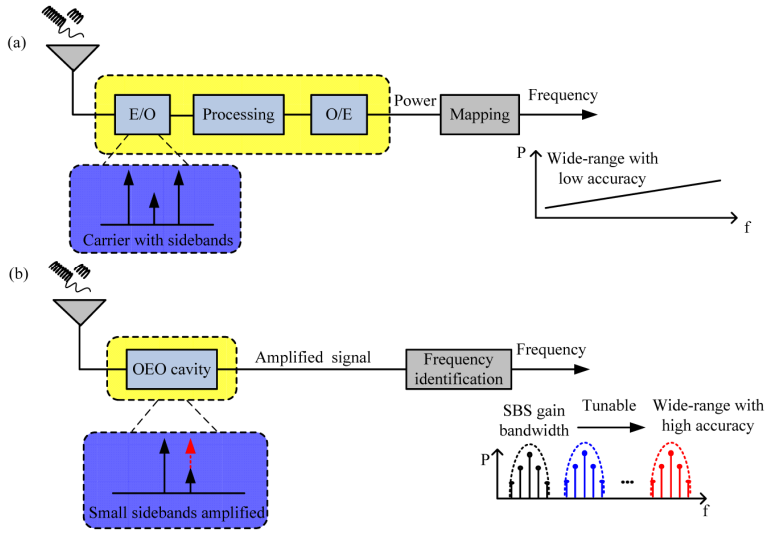

Fig. 1. (a) Conventional photonic RF signals detection and frequency measurement system with power-to-frequency mapping and (b) the here demonstrated photonic RF signal detection and frequency measurement system based on an OEO cavity.

Optics EXPRESS

2. Principle of frequency identification

The conventional RF photonics signal detection and frequency measurement system [9–14] is shown in Fig. 1(a). Strong optical sidebands are used for subsequent optical signal processing techniques. Thus, high RF input power is required in the electro-optical conversion process, which limits the sensitivity of the system. Besides, there is a trade-off between detection range and accuracy since power to frequency mapping is implemented in the whole frequency bands. In our approach, summarized in Fig. 1(b), an optoelectronic oscillator (OEO) cavity is used for detection, which provides gain to the unknown RF signals by matching the oscillation modes. Hence, the sensitivity of the system is greatly improved. Furthermore, the use of tunable and narrow amplification bandwidth of on-chip SBS (tens of MHz) [15] enables a wide frequency range and high accuracy.

The conceptual diagram of our proposed RF signal detection and frequency estimation scheme is shown in Fig. 2, which includes two steps: detecting the signal received from the antenna and estimating the frequency. The key to our approach is the B-OEO with a narrow bandwidth of tens of MHz [16]. The oscillation of the B-OEO is initiated from noise. When the open-loop gain is larger than unity, a noise component travels around the loop, it is amplified and its amplitude increases until it arrives at a stable state. The oscillation mode is selected in the B-OEO by SBS instead of an electrical filter commonly used in conventional OEOs. At the initial state, the gain of the OEO loop is maintained just below the oscillation threshold by controlling the pump power. Being just below threshold makes the OEO very sensitive to a received unknown signal. Once an unknown RF signal is fed into the cavity, it can be distinguished by its relative frequency difference to the cavity modes with the most extreme case being one RF frequency matching the oscillation frequency of the B-OEO. The B-OEO provides gain to the unknown signal that is matching the oscillation mode, which ensures the high sensitivity of the system.

In our scheme, an optical carrier from the signal laser with a frequency of f_s is phase modulated by the RF signal to be detected with a frequency of $f_{detected}$, as shown in Fig. 2(a)I. When the frequency of the upper sideband equals the frequency of the Stokes wave generated by a counter-propagating optical pump, it will be amplified by the SBS process. This will lead to phase-to-intensity modulation conversion, as shown in Fig. 2(a)II. The Brillouin gain is provided by a second laser, the optical pump, with a frequency given by $f_p = f_s + f_{detected} + \Omega_B$ (Ω_B is the SBS frequency shift). By sweeping the frequency of the pump the oscillation frequency is changed due to the central frequency shifting of the SBS gain spectrum and the unknown RF frequency $f_{detected}$ can be identified, as shown in Fig. 2(a) III.

Next, the frequency of the detected RF signal is estimated using power-to-frequency mapping as shown in Fig. 2(b). In order to understand the relation between the frequency of the unknown signal and the RF power change, one can suppose that the frequency of the pump can be gradually changed with the interval of the FSR of the B-OEO. Then the power change at different modes is recorded accordingly as shown in Fig. 2(b). Since the SBS frequency shift is fixed, once the maximum power is obtained, the frequency of the pump at this moment is used to estimate the unknown signal by the frequency difference between the Stokes frequency and the signal laser ($f_{detected} = f_p-\Omega_B-f_s$). Since the tunable range of the pump is large, the unknown signal with different frequency bands can be measured. In ideal conditions, as long as the length of the OEO loop is short enough, the FSR of the cavity is larger than the SBS gain bandwidth. This means there is only one oscillation mode in the SBS gain bandwidth. In this scenario it is easy to get the accurate frequency of the detected RF signal by calculating the frequency difference between the Stokes wave and the signal laser ($f_{detected} = f_p-\Omega_B-f_s$). In our system, an additional erbium-doped fiber amplifier (EDFA) is used to compensate for the insertion loss of the chip to induce OEO oscillation. This increases the length of the OEO cavity and causes the FSR to be smaller than the SBS gain bandwidth. In this case, there are several side modes present besides the main oscillation mode in the SBS gain bandwidth, which increases the uncertainty of the frequency estimation. However, due to

Optics EXPRESS

the narrow bandwidth and hence steep roll-off of the gain profile provided by SBS, the main oscillation mode experiences still more gain than the side modes. Thus, the estimated frequency error of this scheme remains low.

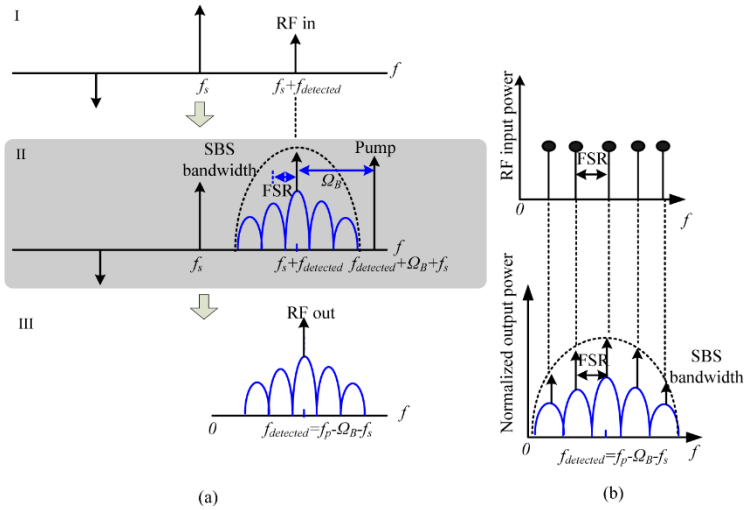

Fig. 2. Conceptual diagram of the proposed photonic RF signal detection and frequency estimation scheme.

3. Experiment

3.1 Designed RF signal detection and frequency estimation system

The experimental setup based on the principle above is shown in Fig. 3. A distributed feedback (DFB) signal laser with the frequency of f_s is first sent into a phase modulator (PM). Then the optical signal is coupled to a highly nonlinear chalcogenide rib waveguide after passing through an optical isolator and a polarization controller (PC2). The isolator here is to avoid back reflections and the PC2 is to maximize the transmission through the chip. The chalcogenide waveguide in our experiment was fabricated using the standard photolithography of an As_2S_3 film deposited on a SiO_2 substrate, as shown in Fig. 3. The rib structure has a cross-section of 2.5 μm × 0.85 μm, which results in an effective mode area of 1.5 μm^2 and a gain factor of the order of 7×10^{-10} m/W [15]. The length of the waveguide is 9 cm and the total insertion loss of the waveguide is about 12.5 dB, including ~4 dB coupling loss per facet and ~0.5 dB/cm propagation loss. Another DFB laser with the frequency of f_P serves as a pump and is coupled from the opposite side to the chip. The use of a boost EDFA and a PC3 is to ensure the strong interaction between the optical pump and the counter-propagating signal to generate a strong acoustic and optical Stokes wave. The amplification of the Stokes wave provides the narrow-band gain response in the B-OEO cavity. The optical signals at port 3 of the circulator is sent to the photodetector via an optical band-pass filter (OBPF) and a low noise EDFA (LN-EDFA). After opto-electrical conversion, the electrical signal is amplified by an electrical amplifier and divided into two paths by electrical coupler 1. One path is for spectrum monitoring by an electrical spectrum analyzer (ESA). The other path couples the unknown RF signal from the antenna and feeds into the RF port of the PM via electrical coupler 2 to close the B-OEO cavity. The use of SBS sideband amplification to achieve phase-to-intensity modulation conversion allows for the use of PM instead of intensity modulator commonly used in OEOs. The PM has a lower insertion loss and is more stable since a direct current bias is not required. Furthermore, making use of the narrow-band selected amplification characteristic of SBS instead of an electrical filter to achieve single mode oscillation increase the tunable frequency range of the system.

Optics EXPRESS

To better understand our RF signal detection and frequency estimation system, the spectrum evolution at different points of the OEO cavity is also shown in Fig. 3. The output of the PM contains an optical carrier and two first-order sidebands, which have identical amplitude and opposite phase, as shown in Fig. 3(b). When the unknown RF signal locates at the Stokes frequency (f_p-Ω_B) of the optical pump, one sideband of the phase modulated signal is amplified by the SBS gain spectrum. Thus, the phase modulation is converted to intensity modulation, as shown in Fig. 3(c). Since the pump signal reflected by the chalcogenide chip is large, an OBPF is used to eliminate the back reflected pump signal. The spectrum at the output of the OBPF is shown in Fig. 3(d). Upon photodetection and feedback to the PM, only the signals in the SBS gain bandwidth are oscillating, and only the unknown RF signal with the frequency equal to the beating frequency between signal laser and Stokes wave ($f_{detected}$ = f_p-Ω_B-f_s) is amplified due to the oscillation of the B-OEO, as shown in Fig. 3(e). Since the frequency of the pump can be tuned arbitrarily, it is easy to sweep the SBS gain spectrum to select the unknown RF signal. Since the gain provided by the oscillation mode and side modes are different, the frequency of the unknown RF signal can be estimated accurately. Note that, in principle, also the SBS loss resonance at the higher frequency side of the pump (f_p + Ω_B) could lead to a conversion from phase to intensity modulation. The Brillouin loss, however, does not play a role in our implementation for the following two reasons: First of all, we use a sharp filter that removes pump back-reflection from the chip facet. Secondly, the OEO loop is operated at a point where the open loop gain only becomes positive when the SBS gain is applied and hence the loss resonance is not oscillating.

Optics EXPRESS

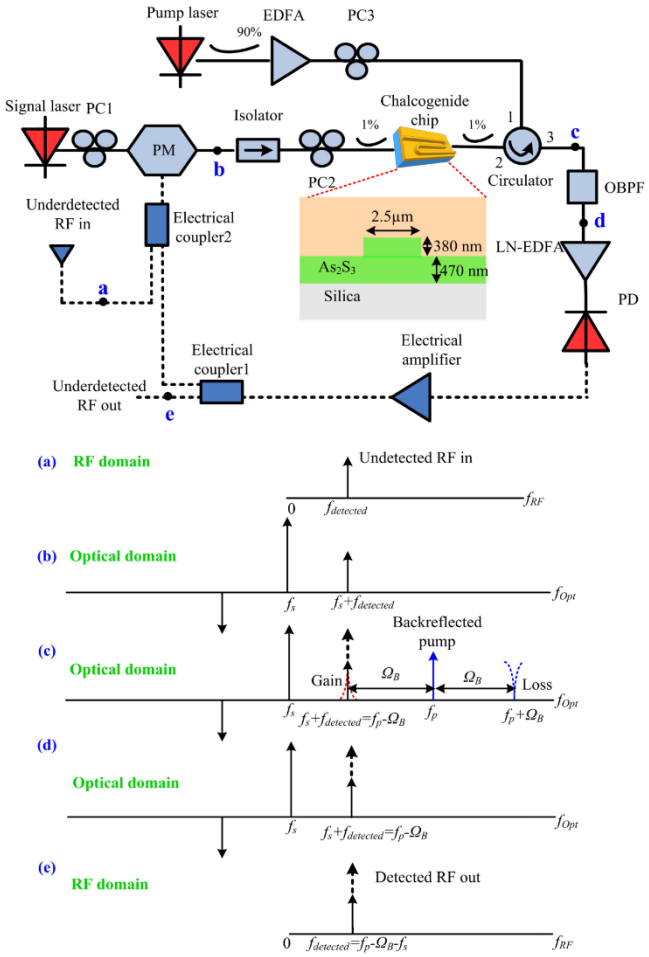

Fig. 3. Experimental setup. PC, Polarization controller; PM, Phase modulator; EDFA, Erbium-doped fiber amplifier; OBPF, Optical band-pass filter; LN-EDFA, Low noise EDFA; PD, Photodetector.

3.2 Experimental results analysis

First, two RF signals are injected into the B-OEO cavity to demonstrate selective RF amplification (inset Fig. 4). In all of our measurements, the frequency of the signal laser is around 193 THz and we adjust the frequency of the pump laser to tune the oscillation frequency between 1.5~40 GHz. Figure 4 shows the measured output spectrum of the B-OEO when two RF signals with the same power of −52 dBm at two different frequencies of 16.129 and 16.131 GHz are injected in the B-OEO. We can see from Fig. 4 that the mode spacing of the B-OEO is 3.4 MHz, which is determined by the length of the cavity. The theoretical mode spacing of the B-OEO loop is c/(nL), where $c = 3 \times 10^8$ m/s is the speed of light in vacuum, n is the effective refractive index of the media, and L is the length of the B-OEO loop. Since the main transmission medium in our B-OEO loop is SMF, the effective index n is around 1.45. The total length of the B-OEO loop is about 55.9 m including 27.4 m of fiber inside the LN-EDFA (Amonics AEDFA-PA-35-B-FA). The theoretical calculated mode spacing is about 3.7 MHz, which is consistent with the experimental result. The output power of RF signal with the frequency equal to the oscillation frequency (16.129 GHz) is −38 dBm, which is amplified by 14 dB, while the output power of the RF signal with the frequency of 16.131 GHz is −65 dBm, which is attenuated by 13 dB since it is not matching the oscillation mode.

Optics EXPRESS

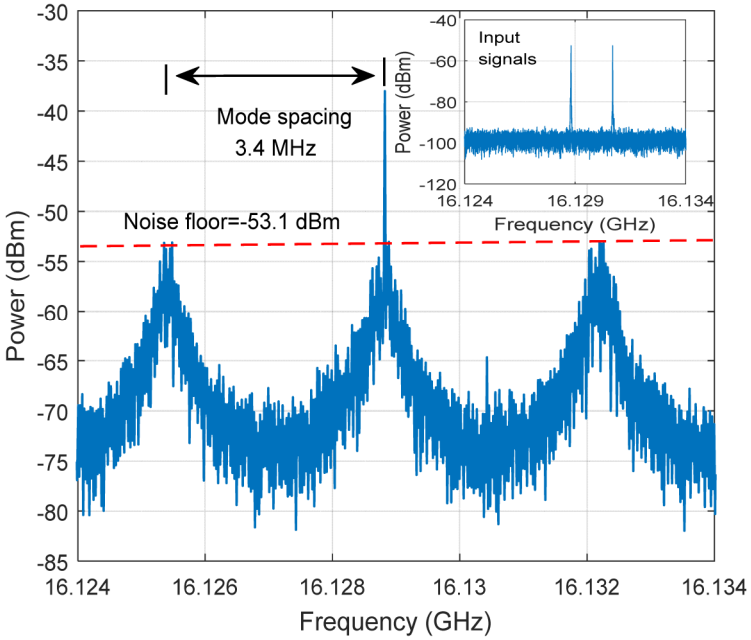

Fig. 4. Measured spectrum of the input (inset) and detected RF signals with the same input power of −52 dBm and frequencies of 16.129 and 16.131 GHz.

Next, the sensitivity of our B-OEO detection scheme is investigated, which determines the lowest power of the RF signal that can be detected. The detection sensitivity of our scheme is not only determined by the cavity mode noise floor (N), but also is determined by the gain of B-OEO for input RF signals (G). In theory, the detection sensitivity can be calculated as N-G in dB. Thus, the cavity mode noise should be kept low and the gain of B-OEO high to maximize the detection sensitivity. In the experiment, we decrease the power of the RF input signal until the detected signal cannot be distinguished from the cavity mode. This measurement determines the lowest possible input power that is still above the cavity noise floor. The measured spectrum as the power of input RF signal decreases from −46 to −67 dBm with the resolution bandwidth of the ESA at 10 kHz is shown in Fig. 5. We can see from Fig. 5 that the cavity mode noise is −53.1 dBm, which is influenced by the optical and electrical amplifier noise and SBS induced amplified spontaneous noise (ASE). The unknown RF signal is above the cavity mode noise until the power of the input signal is −67 dBm, which means the detection sensitivity around 16 GHz frequency is −67 dBm.

Optics EXPRESS

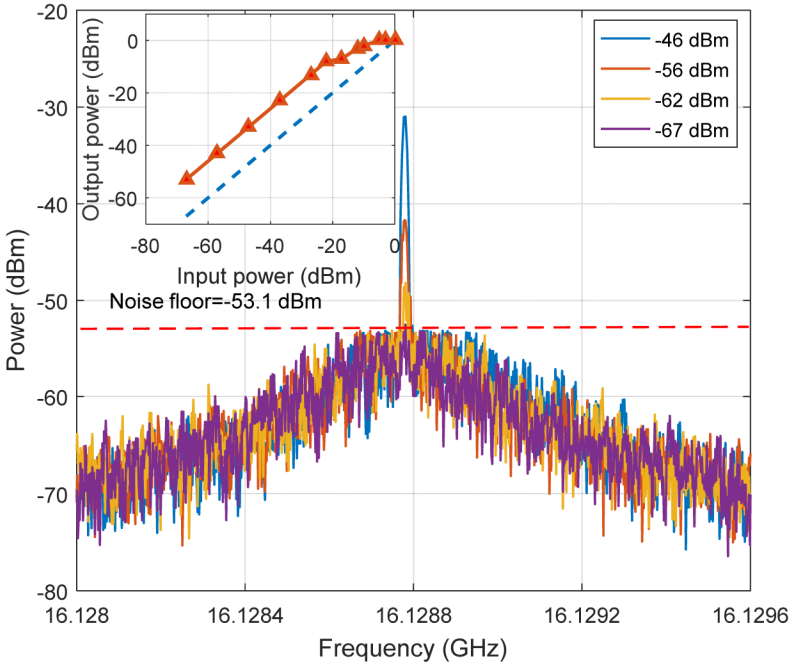

Fig. 5. Measured spectrum with different input RF signal power level at a frequency of 16.129 GHz.

The dynamic range is another important parameter to evaluate the amplification range of the B-OEO for different input RF signal powers. The dynamic range is defined as the difference between the minimum detectable signal power and the maximum detectable signal power before the gain of the unknown signal is saturated. The measured output power as a function of input RF signal power from −67 to 0 dBm is shown in the inset of Fig. 5. The blue line is a linear curve for the case where there is 0 dB gain provided by the B-OEO. We can see that the gain of the unknown signal decreases as the increase of the input RF signal power. When the input RF signal power reaches 0 dBm, there is no gain provided by the B-OEO. This means the gain dynamic range of our scheme at a frequency of around 16 GHz is about 67 dB which is mainly limited by the PM and the electrical amplifier. Note that RF signals that fall in between the oscillating mode and adjacent modes (compare Fig. 5 inset) are not amplified by the loop and are attenuated by the overall insertion loss of the OEO loop. Hence in the power range of interest the RF signals in between the OEO modes are always much lower than the RF signals on resonance and follow the same trend in the unsaturated regime.

In order to demonstrate the wide detection range of the proposed B-OEO approach, the selective amplification for a frequency of around 40 GHz is also measured, as shown in Fig. 6. The frequency of the pump laser is tuned to a frequency difference between signal laser and Stokes signal of 39.379 GHz, which determines the oscillation frequency of the B-OEO. When the RF signals with the same power of −52 dBm at the frequency of 39.379 and 39.381 GHz are injected in the B-OEO, the output power of RF signal with the frequency equals to the oscillation frequency (39.379 GHz) is −40.7 dBm, which is amplified by 11.3 dB. On the other hand, the output power of the 39.381 GHz RF signal that does not match the oscillation mode is −64 dBm, an attenuation of 12 dB compared to the input power.

Optics EXPRESS

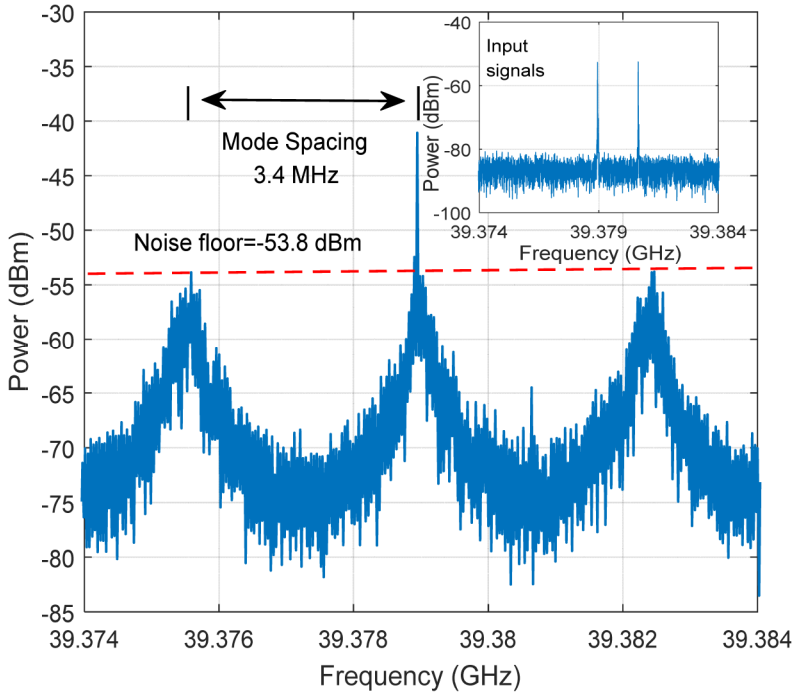

Fig. 6. Measured spectrum of the input and detected RF signals with the same input power of −52 dBm at the frequency of 39.379 and 39.381 GHz.

Furthermore, the detection sensitivity and gain dynamic range for a frequency around 40 GHz are investigated. As shown in Fig. 7, the measured spectrum as the power of input RF signal decreased from −42 to −65 dBm with the resolution bandwidth of the ESA at 10 KHz is recorded. The detection sensitivity for 40 GHz frequency is about −65 dBm when the measured cavity mode noise is −53.8 dBm, which is more than 30 dB higher than that of the previous scheme [5]. The detection sensitivity for 40 GHz frequency band has slightly changed compared with that for 16 GHz due to the performance limitations of the available equipment. When the input RF signal power reaches −1 dBm, the gain for the unknown RF signal provided by the B-OEO is 0, which means the gain dynamic range of our scheme around 40 GHz frequency is about 64 dB. Thus, the detection performance for the 40 GHz system is almost not deteriorated compared with that for the 16 GHz system.

Optics EXPRESS

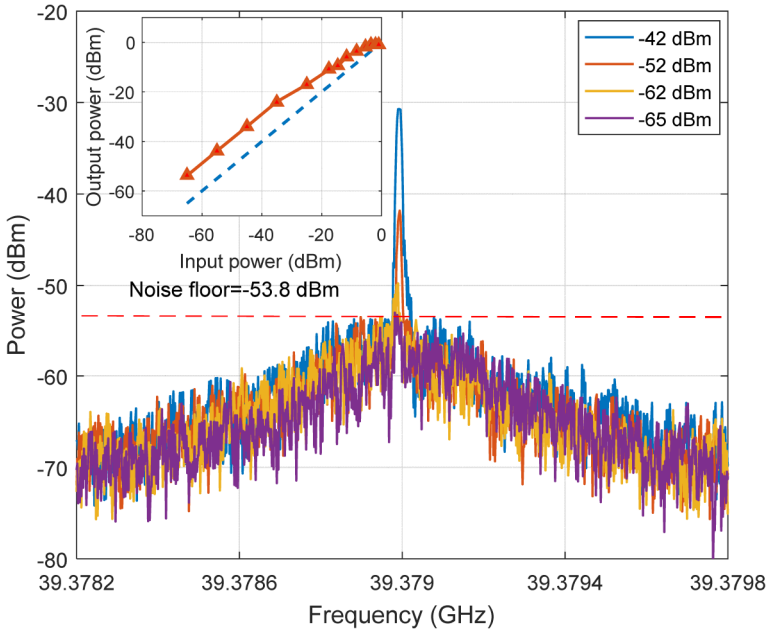

Fig. 7. Measured spectrum with different input RF signal power at the frequency of 39.379 GHz.

The gain for unknown RF signal from 1.5 to 40 GHz with the input power of −56 dBm is measured in order to show the wide detection range and high sensitivity of the proposed B-OEO scheme. As shown in Fig. 8, the gain for 13 GHz RF input signal is maximum and all the gain values from 1.5 to 40 GHz are higher than 10 dB. Since the gain values for different frequencies are measured with the same cavity mode noise, our scheme can achieve 1.5-40 GHz detection range with high sensitivity. This is the widest frequency detection range achieved by the chip-based system due to the good frequency tunability of on-chip SBS. The broader frequency detection range can be achieved by using the same optoelectronic devices with higher frequency. It is noted from Fig. 8 that the gain for different frequencies is not flat. This variation is mainly due to the frequency response of the OEO cavity caused by the frequency-dependent half-wave voltage of the PM, and the different frequency responses of the electrical amplifier, electrical coupler and electrical cable.

Optics EXPRESS

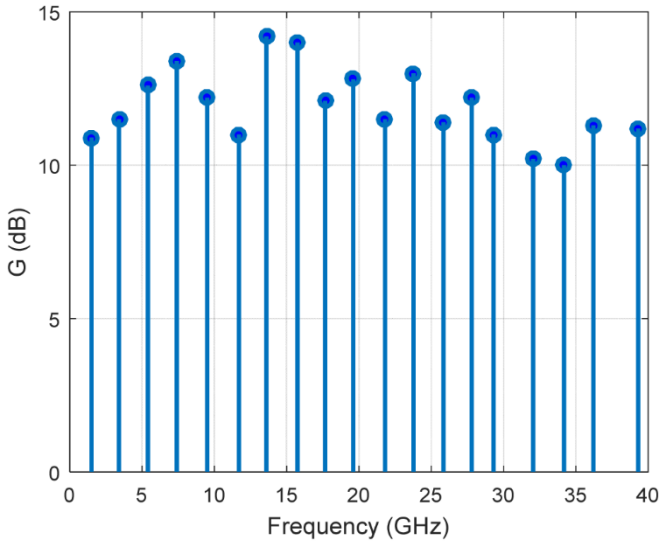

Fig. 8. Gain for RF signals at different frequencies.

Finally, estimation error for different frequency bands are investigated. First, the frequency difference between the pump and signal laser is set at 9.2257 GHz. Thus, the B-OEO oscillates at the frequency of 1.5307 GHz (f_p-Ω_B-f_s) since the SBS frequency shift of the waveguide is measured to be $\Omega_B \approx 7.695$GHz. Then, an RF signal at the oscillation frequency is input to the B-OEO, and the corresponding output power is measured. We change the input RF signal frequency to adjacent side modes frequencies (1.5239 GHz, 1.5273 GHz, and 1.5241 GHz), and the corresponding output power are measured with the same input power as shown in Fig. 9. Here, we assume that we need to have at least 1dB output power difference to distinguish the main oscillation mode from the adjacent modes. We can see from Fig. 9 that for the unknown RF signal with the frequencies of 5.2617 GHz, 13.4908 GHz, 29.4131 GHz, 31.7145 GHz, and 39.4831 GHz, the power at the oscillation mode is at least 1.5 dB higher than that at the adjacent modes. Thus, we can distinguish the unknown signal at the oscillation mode from the side modes for these frequency bands. For the unknown RF signal with the frequencies of 1.5307 GHz, 9.3488 GHz, 17.6057 GHz, 21.6893 GHz, and 25.7869 GHz, although there is only little power difference between the oscillation mode and the adjacent mode, the power at the oscillation mode is still at least 1.4 dB higher than that at the second adjacent modes. Thus, the frequency uncertainty of the proposed B-OEO approach with 1.5 to 40 GHz range is about ± 3.4 MHz, which is lower than that of the previous schemes [12,13].

Optics EXPRESS

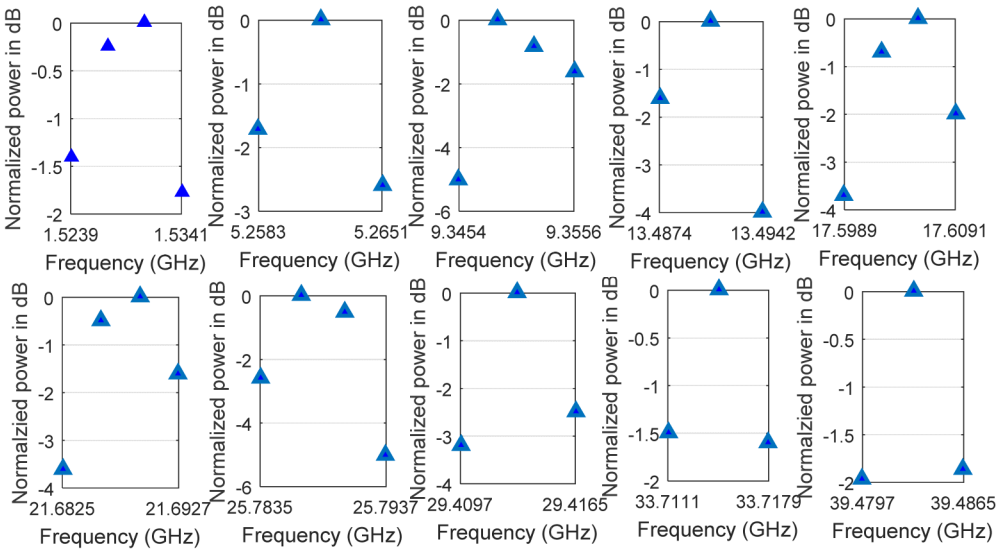

Fig. 9. Normalized output RF signal power oscillation mode and side modes for different frequency bands.

4. Discussion

The detection sensitivity of the B-OEO approach is influenced by the cavity mode noise of the system. In our experiment, one optical amplifier and two electrical amplifiers are used to compensate the losses caused by the insertion loss of the chalcogenide chip and the additional OBPF to suppress back reflection from the chip. The introduced amplifier noise increases the cavity mode noise, leading to the reduction of sensitivity of the B-OEO. However, these challenges are not fundamental to the scheme and can be overcome by on-chip tapers [14] or photonic wire bonding [17], which reduces both the insertion loss and back reflection of the chip. Moreover, we would note that the position of the LN-EDFA that is required in our current implementation is important for the optimization of the detection sensitivity of the system. If the LN-EDFA is placed before the PM, the noise of the system is lower. However, in this case the gain of the B-OEO cavity is not high enough to oscillate due to the loss of the chalcogenide waveguide. If the LN-EDFA is placed after the chip or before the OBPF, the reflected pump from the chip will compete for the gain of the LN-EDFA since its power is higher than that of the optical carrier, which decreases the gain of the OEO cavity. Thus, the detection sensitivity for our B-OEO is optimum when the LN-EDFA is put after the OBPF.

The RF frequency is measured by calculating the frequency difference between the signal laser and the peak of the SBS gain spectrum. For practical applications that require fast RF detection capabilities, a swept wavelength system can be used as the pump or probe.

Individual pump and probe lasers were used for this demonstration requiring ultra-stable laser sources as relative wavelength drift of the pump and probe lasers can affect the detection accuracy. In order to further improve the stability of the two lasers B-OEO system, a fixed phase difference between the signal light and the pump light can be achieved by phase control methods. These techniques can greatly reduce the relative frequency change caused by wavelength drift [6]. Furthermore, our scheme can be also implemented using a single laser system to eliminate the relative wavelength drift. For a single laser system, the optical carrier for the pump and probe sides are generated by the same laser. A phase modulator and a tunable OBPF can be used to generate an optical single sideband signal [18], which can be used as the pump signal. Through sweeping the RF reference signal frequency that generates the sidebands, the frequency of the pump signal can be finely controlled.

Optics EXPRESS

In order to further reduce the estimation error, ideally only one oscillator mode would be within the SBS gain spectrum. This can be achieved by either shortening the cavity to increase the free spectrum range (FSR) of the OEO or by reducing the SBS gain bandwidth. In order to reduce the cavity length, we can use a semiconductor optical amplifier (SOA) instead of the EDFA to minimize the length of fiber in the cavity or use a chip with lower losses to remove the requirement of an additional EDFA. In the long term, a fully integrated B-OEO system on a chip would allow for a very short cavity length. The SBS gain bandwidth, on the other hand, can be reduced via the superposition of an SBS gain with two SBS loss spectra [19]. This method allowed the reduction of the SBS gain bandwidth to 3.4 MHz.

Ultimately, it is possible to monolithically integrate all critical components of the B-OEO system on a chip, reducing the cavity length and the overall footprint of the system, greatly improving the overall performance of the scheme. For the laser, low-loss heterogeneous III-V/silicon [20] and hybrid III-V/Si_3N_4 [21] lasers have recently been demonstrated on chip. Different electro-optical modulators based on silicon [22], indium phosphide [23], polymers [24] and plasmonics [25] are available. All these approaches have shown to be scalable and exhibit distinct performance merits, like low drive voltages (InP, polymer), ultra-high bandwidths (polymer, plasmonics) and small footprints (Si, plasmonics) and can be integrated with CMOS electronics (Si). Concerning the SBS waveguide, a hybrid chalcogenide-on-silicon structure or silicon waveguides can be used as Brillouin net gain in silicon, which has been demonstrated recently [26]. High power and high-speed photodetectors are also available on chip [27]. Finally, integrated optical circulators on silicon that are electrically driven and dynamically reconfigurable can be also obtained [28].

5. Conclusion

We have presented the first RF signal detection and frequency estimation system using a B-OEO based on on-chip SBS. The gain for the unknown RF signal provided by the opto-electrical oscillation ensures the high sensitivity. The narrow bandwidth selective amplification of SBS solves the trade-off between the wide detection range and high accuracy. RF signals from 1.5 to 40 GHz as low as −67 dBm are detected with an estimation error of ± 3.4 MHz. With all the required components of our scheme already demonstrated in an integrated platform, our demonstration opens the way for a reconfigurable, monolithically integrated RF signal detection and frequency estimation system with tens of GHz measurement range, sub-megahertz accuracy, and negative tens of dBm sensitivity in a silicon chip.

Funding

Australian Research Council (ARC) Linkage grant (LP170100112) with Harris Corporation. U.S. Air Force (USAF) through AFOSR/AOARD (FA2386-16-1-4036); U.S. Office of Naval Research Global (ONRG) (N62909-18-1-2013).

Acknowledgment

This work was performed in part at the ACT node of the Australian National Fabrication Facility, a company established under the National Collaborative Research Infrastructure Strategy to provide nano- and micro-fabrication facilities for Australia's researchers.

References

1. C. Wang, F. Haider, X. Gao, X. You, Y. Yang, D. Yuan, H. M. Aggoune, H. Haas, S. Fletcher, and E. Hepsaydir, "Cellular architecture and key technologies for 5G wireless communication networks," IEEE Commun. Mag. **52**(2), 122–130 (2014).
2. P. S. Devgan, V. J. Urick, and K. J. Williams, "Detection of low-power RF signals using a two laser multimode optoelectronic oscillator," IEEE Photonics Technol. Lett. **24**, 857–859 (2012).

Optics EXPRESS

3. A. M. Sardarabadi, A. J. van der Veen, and A. J. Boonstra, "Spatial Filtering of RF Interference in Radio Astronomy Using a Reference Antenna Array," IEEE Trans. Signal Process. **64**(2), 432–447 (2016).
4. W. B. Sullivan, "Instantaneous frequency measurement receivers for maritime patrol," J. Electron. Defence **25**, 55–62 (2002).
5. H. Emami, M. Hajihashemi, S. E. Alavi, A. S. M. Supaat, and L. Bui, "Microwave photonics instantaneous frequency measurement receiver based on a Sagnac loop," Opt. Lett. **43**(10), 2233–2236 (2018).
6. G. Wang, T. Hao, W. Li, N. Zhu, and M. Li, "Detection of wideband low-power RF signals using a stimulated Brillouin scattering-based optoelectronic oscillator," Opt. Commun. **439**, 133–136 (2019).
7. Y. Shao, X. Han, M. Li, and M. Zhao, "RF signal detection by a tunable optoelectronic oscillator based on a PS-FBG," Opt. Lett. **43**(6), 1199–1202 (2018).
8. J. Niu, S. Fu, K. Xu, J. Zhou, S. Aditya, J. Wu, P. P. Shum, and J. T. Lin, "Instantaneous microwave frequency measurement based on amplified fiber-optic recirculating delay loop and broadband incoherent light source," J. Lightwave Technol. **29**(1), 78–84 (2011).
9. D. Marpaung, "On-chip photonic-assisted instantaneous microwave frequency measurement system," IEEE Photonics Technol. Lett. **25**(9), 837–840 (2013).
10. J. S. Fandiño and P. Muñoz, "Photonics-based microwave frequency measurement using a double-sideband suppressed-carrier modulation and an InP integrated ring-assisted Mach-Zehnder interferometer filter," Opt. Lett. **38**(21), 4316–4319 (2013).
11. L. Liu, F. Jiang, S. Yan, S. Min, M. He, D. Gao, and J. Dong, "Photonic measurement of microwave frequency using a silicon microdisk resonator," Opt. Commun. **335**, 266–270 (2015).
12. M. Burla, X. Wang, M. Li, L. Chrostowski, and J. Azaña, "Wideband dynamic microwave frequency identification system using a low-power ultracompact silicon photonic chip," Nat. Commun. **7**(1), 13004 (2016).
13. M. Pagani, B. Morrison, Y. Zhang, A. Casas-Bedoya, T. Aalto, M. Harjanne, M. Kapulainen, B. J. Eggleton, and D. Marpaung, "Low-error and broadband microwave frequency measurement in a silicon chip," Optica **2**(8), 751–756 (2015).
14. H. Y. Jiang, D. Marpaung, M. Pagani, K. Vu, D. Y. Choi, S. J. Madden, L. S. Yan, and B. J. Eggleton, "Wide-range, high-precision multiple microwave frequency measurement using a chip-based photonic Brillouin filter," Optica **3**(1), 30–34 (2016).
15. M. Merklein, A. Casas-Bedoya, D. Marpaung, T. F. S. Buttner, M. Pagani, B. Morrison, I. V. Kabakova, and B. J. Eggleton, "Stimulated Brillouin Scattering in Photonic Integrated Circuits: Novel Applications and Devices," IEEE J. Sel. Top. Quantum Electron. **22**(2), 336–346 (2016).
16. M. Merklein, B. Stiller, I. V. Kabakova, U. S. Mutugala, K. Vu, S. J. Madden, B. J. Eggleton, and R. Slavík, "Widely tunable, low phase noise microwave source based on a photonic chip," Opt. Lett. **41**(20), 4633–4636 (2016).
17. N. Lindenmann, G. Balthasar, D. Hillerkuss, R. Schmogrow, M. Jordan, J. Leuthold, W. Freude, and C. Koos, "Photonic wire bonding: a novel concept for chip-scale interconnects," Opt. Express **20**(16), 17667–17677 (2012).
18. M. Shi, L. Yi, W. Wei, and W. Hu, "Generation and phase noise analysis of a wide optoelectronic oscillator with ultra-high resolution based on stimulated Brillouin scattering," Opt. Express **26**(13), 16113–16124 (2018).
19. S. Preußler, A. Wiatrek, K. Jamshidi, and T. Schneider, "Brillouin scattering gain bandwidth reduction down to 3.4MHz," Opt. Express **19**(9), 8565–8570 (2011).
20. M. A. Tran, D. Huang, T. Komljenovic, J. Peters, A. Malik, and J. E. Bowers, "Ultra-Low-Loss Silicon Waveguides for Heterogeneously Integrated Silicon/III-V Photonics," Appl. Sci. (Basel) **8**(7), 1139–1150 (2018).
21. Y. Fan, R. M. Oldenbeuving, C. G. Roeloffzen, M. Hoekman, D. Geskus, R. G. Heideman, and K. J. Boller, "290 Hz intrinsic linewidth from an integrated optical chip-based widely tunable InP-Si3N4 hybrid laser.," In CLEO: 2017 Paper Digest JT5C.9, (2017).
22. Q. Xu, B. Schmidt, S. Pradhan, and M. Lipson, "Micrometre-scale silicon electro-optic modulator," Nature **435**(7040), 325–327 (2005).
23. Y. Ogiso, J. Ozaki, Y. Ueda, N. Kashio, N. Kikuchi, E. Yamada, H. Tanobe, S. Kanazawa, H. Yamazaki, Y. Ohiso, T. Fujii, and M. Kohtoku, "Over 67 GHz bandwidth and 1.5 V InP-based optical IQ modulator with n-i-p-n heterostructure," J. Lightwave Technol. **35**(8), 1450–1455 (2017).
24. M. Lee, H. E. Katz, C. Erben, D. M. Gill, P. Gopalan, J. D. Heber, and D. J. McGee, "Broadband modulation of light by using an electro-optic polymer," Science **298**(5597), 1401–1403 (2002).
25. C. Haffner, D. Chelladurai, Y. Fedoryshyn, A. Josten, B. Baeuerle, W. Heni, T. Watanabe, T. Cui, B. Cheng, S. Saha, D. L. Elder, L. R. Dalton, A. Boltasseva, V. M. Shalaev, N. Kinsey, and J. Leuthold, "Low-loss plasmon-assisted electro-optic modulator," Nature **556**(7702), 483–486 (2018).
26. R. Van Laer, B. Kuyken, D. Van Thourhout, and R. Baets, "Interaction between light and highly confined hypersound in a silicon photonic nanowire," Nat. Photonics **9**(3), 199–203 (2015).
27. A. Beling, A. S. Cross, M. Piels, J. Peters, Q. Zhou, J. E. Bowers, and J. C. Campbell, "InP-based waveguide photodiodes heterogeneously integrated on silicon-on-insulator for photonic microwave generation," Opt. Express **21**(22), 25901–25906 (2013).
28. D. Huang, P. Pintus, C. Zhang, P. Morton, Y. Shoji, T. Mizumoto, and J. E. Bowers, "Dynamically reconfigurable integrated optical circulators," Optica **4**(1), 23–30 (2017).